SEMESTA TEKNIKA
E-ISSN: 2502 - 5481 P-ISSN: 1411 - 061X
Semesta Teknika
Vol. 27, No. 2, 213-222, November 2024
DOI: https://doi.org/10.18196/st.v27i2.24748

The effect of welding time on the tensile load capacity of dissimilar-metal stainless steel-carbon steel TIG-Spot welded joint

Aris Widyo Nugroho *, Hadi Prayitno, Muhammad Budi Nur Rahman
Department of Mechanical Engineering, Faculty of Engineering, Universitas Muhammadiyah Yogyakarta

Jl. Brawijaya, Kasihan, Tamantirto, Kasihan, Bantul, Daerah Istimewa Yogyakarta, Indonesia

* Corresponding author email: ariswidyo.nugroho@umy.ac.id

Keywords:
Spot-TIG welding;
SS 430;
Carbon steel;
Dissimilar joint.

Abstract

This study examines the influence of welding time on the tensile load capacity of spot TIG welds using stainless steel and low carbon steel plates (100 mm × 30 mm × 0.8 mm) as per AWS D8.9 standards. A constant welding current of 90 A was applied, with 2-, 3-, 4-, and 5-seconds welding times. Tensile properties, microstructure, and hardness were analyzed using a universal tensile machine, an optical microscope, a scanning electron microscope, and a Vickers hardness tester. Results show that the tensile load capacity increases with welding time, peaking at 4 seconds (≈4300 N), before dropping significantly at 5 seconds (≈4000 N) due to overheating, which weakens the joint. The findings highlight the critical role of optimizing welding time to maximize joint strength while preserving the material's microstructure. Overextended welding times compromise performance, emphasizing the balance required for achieving durable welds.

INTRODUCTION

Resistance spot welding (RSW) is the predominant method for joint thin sheet metals in the automobile sector (Zhou & Cai, 2014). Nevertheless, when access to both sheet metal surfaces is unattainable, which is essential for resistance spot welding, specific intricate applications pose difficulties. In such scenarios, one-sided TIG-spot welding is a suitable approach for joining metals under challenging conditions. It enables the formation of robust and lasting welds by applying localised heat. Fusing incompatible metals, including carbon steel and stainless steel, is a particular application of TIG spot welding that entails distinct problems and considerations. TIG welding for combining dissimilar metals is possibly utilised in industries where various qualities are required, hence cutting costs and eliminating the necessity for expensive and uncommon materials (Echezona et al., 2021; K. Kumar et al., 2018). Their demand is rising in automotive, aerospace, and chemical sectors (Singh et al., 2013). Challenges encompass the movement of carbon atoms, thermal expansion discrepancies, and electrochemical properties changes.

TIG spot welding has numerous benefits for the fusion of dissimilar metals (Madesh et al., 2022). This approach utilises a localised heat source to melt and fuse metals, generating less thermal tension than the flow technique, hence diminishing stress concentration at the weld site(A. Kumar et al., 2018). The procedure involves placing the metal sheets in proximity and exerting pressure to form a robust joint. A tungsten electrode transmits electric current to the weld zone, while an inert gas shield, usually argon, inhibits oxidation and contamination of the weld area. Multiple criteria must be evaluated for the successful TIG-spot welding of dissimilar metals (Shrivas et al., 2020). This encompasses selecting the appropriate welding parameters, including current, voltage, and time, which are crucial for establishing a robust and enduring junction. The selection of filler material is essential to provide compatibility between the different metals and to enhance the mechanical qualities of the weld. In addition, by optimizing welding time, industries can achieve a balance between productivity, material integrity, and operational efficiency, fostering innovation and competitiveness

Nugroho *et al.* (2024) studied the impact of different welding currents on the tensile load-bearing capability of dissimilar joints of carbon steel and stainless-steel sheets welded by TIG spot welding. The study examined several welding currents (70, 80, 90, and 100 A), revealing that elevated currents enhanced tensile load capacity owing to improved penetration and fusion. The welding procedure caused grain coarsening in the heat-affected zone (HAZ), rendering it more brittle and susceptible to pullout failure under stress in the stainless-steel sheet. In addition, Faozi (2015) investigated the influence of electric current and welding time on the mechanical properties of TIG spot-welded joints composed of SS400 and AA 5083 materials. Argon served as the shielding gas. Augmenting the current and welding time enhances the load-bearing capacity but diminishes hardness due to elevated heat input, which leads to delayed cooling and an enlarged heat-affected zone grain size. A separate study examines the mechanical properties of joints produced using both RSW and TIG-spot welding on dual-phase steel, indicating that junctions with a nugget diameter above 4 mm had a load-bearing capability surpassing the minimum requirement. The association between microstructure and hardness is demonstrated for both RSW and TIG-spot welded joints, with TIG-spot welds exhibiting somewhat lower load-bearing capacity than RSW. Nonetheless, the joint strength is sufficient and satisfies application requirements (Rajak et al., 2023). Furthermore, variables such as current, gas flow rate, and electrode gap affect the tensile strength of different AA5052 and AA6061 joints, with optimal parameters influencing strain rate and minimising inclusions (Shrivas et al., 2020).

The literature study suggests that the feasibility of TIG spot welding for weld bonding necessitates additional examination. In the current operation, TIG spot weld bonding was employed to form weld bindings between different metals, specifically carbon steel and stainless steel. Carbon steel and stainless steel are two separate metals with unique properties and characteristics. Carbon steel's elevated tensile strength and affordability make it appropriate for structural applications. Conversely, stainless steel has remarkable corrosion resistance and hygiene, rendering it an optimal material for applications where sanitation and durability are paramount (Mallick, 2020). Among several process factors, weld current was identified as a critical variable, and its operational range was established through a series of pilot trials. This study aimed to examine the impact of welding time factors on the bearing load capacity of the joint. The fracture mode was also reviewed to provide a comprehensive understanding of the failure mechanisms that influence the weld's performance under tensile loads.

RESEARCH METHODS

Carbon steel and AISI 430 stainless steel sheets, each having a thickness of 0.8 mm, were utilised for the TIG spot welding junction. The sheets were subsequently cut to dimensions of 100 mm in length and 30 mm in breadth, as seen in Figure 1a. An adjustable variable spot-welding device, model EWM 351 Tetrix, with a capacity of 17.7 kVA, was utilised. The sheets' chemical composition was assessed using a spectrometer.

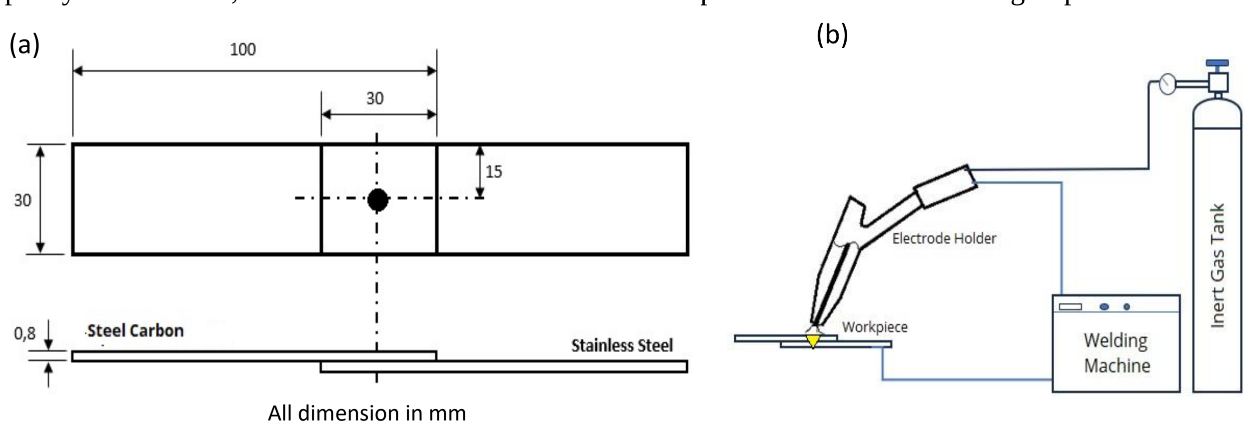

FIGURE 1*. (a) The dissimilar welding joint of carbon steel-stainless steel with spot TIG welding, (b) TIG-spot welding processing*

An optical emission spectrometer, model Thermo ARP 3560 OES, manufactured by Analytical West, was utilised for chemical analysis. The chemical composition of the carbon steel consisted of 0.03 wt% C, 0.19 wt% Mn, 0.03 wt% Si, 0.01 wt% P, 0.009 wt% S, with the remainder being Fe. The chemical composition of the AISI 430 stainless steel sheet comprises 0.1 wt% C, 1 wt% Mn, 0.03 wt% P, 0.02 wt% S, 0.8 wt% Si, 16.9 wt% Cr, with the remainder being Fe. TIG spot welding was employed to facilitate weld bonding. An EWM 351 Tetrix AC/DC power source was utilised alongside an air-cooled TIG torch fitted with a 3 mm diameter tungsten electrode to fabricate weld bonds. The welding procedure was executed at the lap joints, with the carbon steel plate positioned above the stainless steel plate. Figure 1b illustrates the schematic diagram of the TIG spot welding process.

The welding procedure was conducted at various welding times of 2, 3, 4 and 5 seconds at 90 A welding current. Each welding time parameter technique was performed on five specimens. The tensile load-bearing capacity (TLBC) test specimens are depicted in Figure 1(a) and conform to the AWS D9.9-97 standard. The experiments utilised a universal testing machine, Instron 3367, with the maximum force applied to the weld before failure considered the peak load. The specimens undergo tensile shear loading. Each TLBC test was performed thrice, and the mean of these three tests was reported for mechanical property values. An Olympus-type optical microscope model BX53M was utilised to examine the microstructure of the base metal (BM), heat-affected zone (HAZ), and fusion zone (FZ) by scanning electron microscopy (SEM). ImageJ, an open-source software, was utilised for the measuring of image analysis dimensions. The microstructure of the welded connection was examined using a HITACHI-type SEM SU3500 in conjunction with EDS. EDS analysis was employed to assess the quality of the resistance spot welds formed. The hardness of each welding zone was measured using the Mitutoyo model HM-100.

RESULTS AND DISCUSSION

Figure 2a illustrates welded joints employing TIG spot welding, with low carbon steel positioned at the top and stainless steel at the bottom. The top view of the weld nugget at four different welding times is illustrated in Figure 2b.

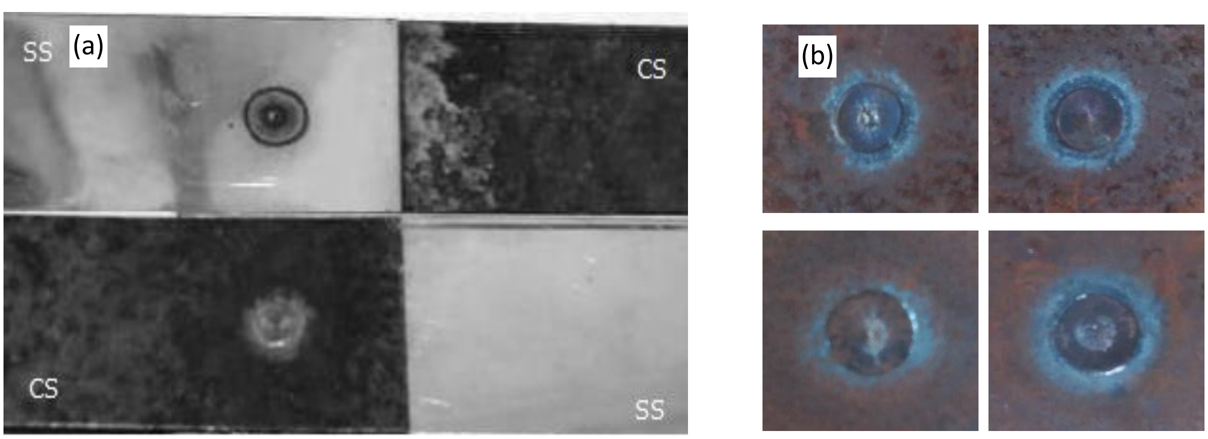

FIGURE 2*. (a) The dissimilar welding joint of carbon steel-stainless steel with spot TIG welding, (b) top view of weld nugget at various welding time*

The workpiece experiences an increased heat input because of a longer welding time. The molten pool and weld nugget area are larger due to the increased energy density, which enables the base metal to undergo more melting and fusion (Akkaş et al., 2016). Increasing the welding time increases the energy input, enabling a deeper penetration of the base metal. The weld nodule has a larger cross-sectional area proportional to the weld bond diameter due to the increased penetration depth (K. Kumar et al., 2018; Lippold & Kotecki, 2005). Furthermore, the tungsten electrode's geometry influences the heat concentration in TIG spot welding. The electrode tip may become larger and more rounded for a longer time as a result of increased heat dissipation.

This can lead to a heat-affected zone that is both larger and more significant, which in turn contributes to a larger weld nugget area (Lippold & Kotecki, 2005).

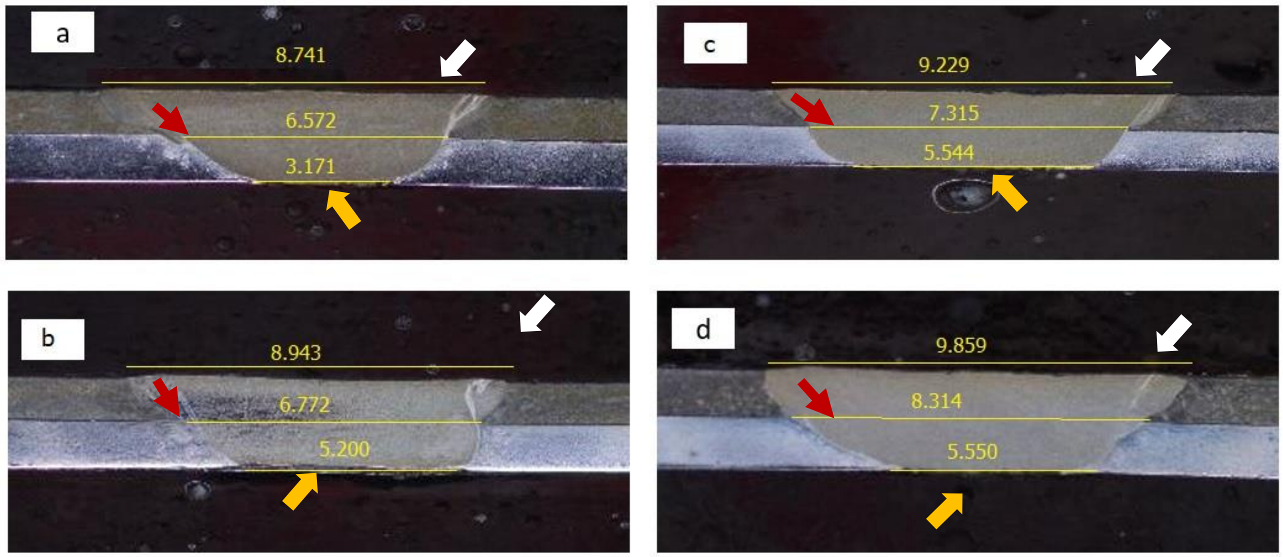

FIGURE 3. *Macrograph of dissimilar TIG spot welding joints in stainless steel 430 and carbon steel for each welding time 2 s (a), 3 s (b), 4 s (c) and 5 s (d)*

Under the experimental design, TIG spot welding was implemented to establish weld bonding. The weld bonds produced for all process parameter values are illustrated in macroscopic images of a few selected specimens in Figure 3. At the macroscopic level, the weld bond was devoid of surface defects (white arrow and orange arrow). The size of the weld bond was measured at the interface of the two sheets (refer to the red arrows). The images depict cross-sections of TIG-spot welded joints, revealing the impact of varying welding times on the weld zone's size and shape. The welding width and penetration depth increase progressively from Figure 3a to Figure 3d, suggesting that higher welding time creates larger weld zones with greater width and depth. White arrows indicate that the weld area on the upper plate expands to a greater extent as the welding time increases, in addition to the increase in the weld bond. Increasing a balanced weld with appropriate depth and width (such as in Figure 3c) may enhance mechanical interlocking and bonding between materials. However, Figure 3d shows the shape of a surface weld pool that is excessively wide compared to its penetration.

The HAZ and FZ microstructures and the BM of CS and SS, are depicted in Figure 4. Although the CS is composed of a ferrite matrix and a small amount of distributed cementite (Pouranvari, 2011), as illustrated in Figure 4a, the BM microstructure of the AISI 430 under investigation is entirely ferritic, with a few carbides (Alizadeh-Sh et al., 2014). Thermal cycling is a phenomenon that occurs during welding and is characterized by a temperature gradient that varies across various zones. The microstructure of TIG-spot welding is typically represented in Figure 4a, which comprises three zones: the fusion zone (FZ), the heat-affected zone (HAZ), and the base metal (BM). The FZ's microstructure is contingent upon its hardening capacity and cooling rate, as it is subjected to temperatures that exceed the steel's melting point. The HAZ is classified into three categories based on peak temperatures above or below critical phases, as stated by Rajak et al. (2023). These categories are upper critical HAZ (UCHAZ), inter-critical HAZ (ICHAZ), and sub-critical HAZ (SCHAZ). The welding thermal cycling does not influence the BM. UCHAZ is further classified into fine-grained heat-affected zone (FGHAZ) and coarse-grained heat-affected zone (CGHAZ). Grain growth is restricted by the lower highest temperature in FGHAZ than in CGHAZ. The line profiles (see blue arrows) of Fe and Cr in CS sheet, as illustrated in Figs. 4b, were analyzed using EDS, and the welding area was also examined. An increase in Cr contents was observed in the direction of the carbon steel through the weld nodule, while the iron content was in the opposite direction. This implies that the CS and SS430 have been fused in FZ.

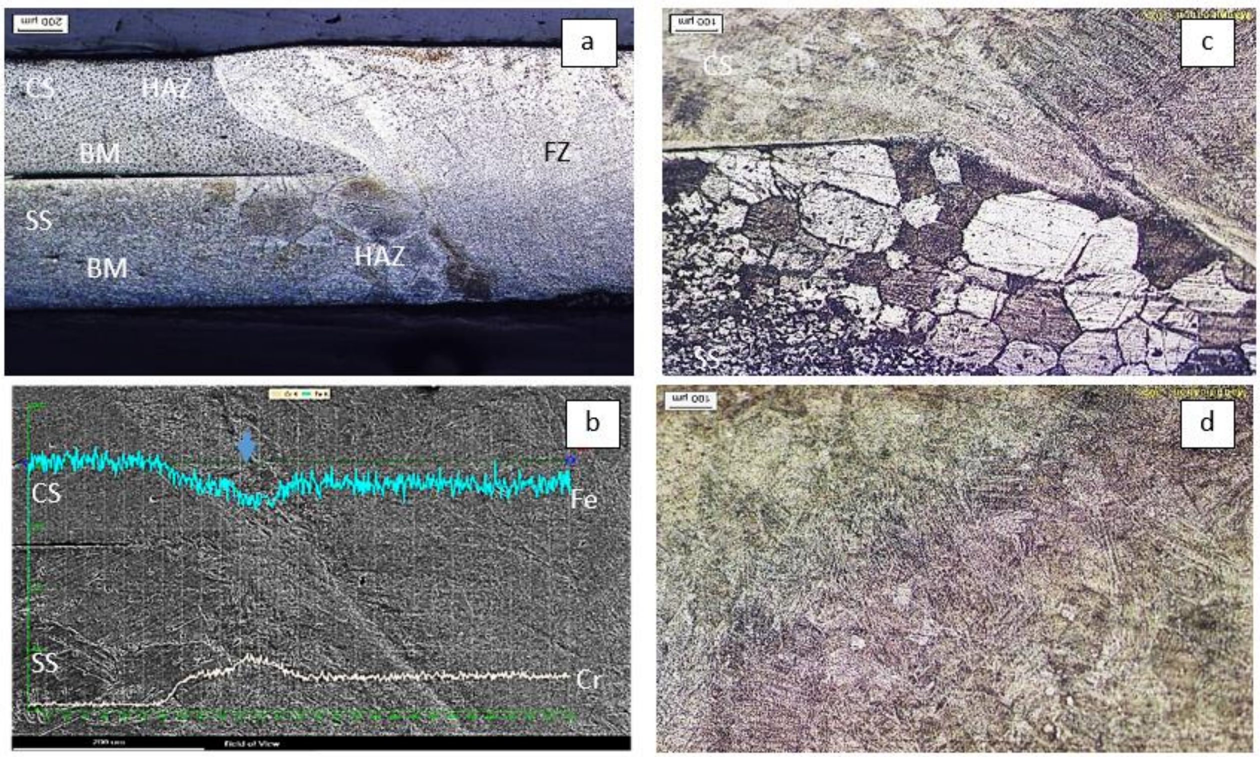

FIGURE 4. *Micrograph of dissimilar TIG spot welding joints (a) line analysis using SEM of the dissimilar joint (b) Optical micrograph of : HAZ of stainless steel 430 welded at 2 second welding time (c) FZ microstructure welded at 2 second (d)*

Alizadeh-Sh et al. (2014) determined that, according to the pseudo-diagram of Fe-Cr-C (Lippold & Kotecki, 2005), the area adjacent to the fusion zone boundary of the stainless steel plate displays a complete δ-ferrite microstructure. A rapid cooling rate inhibits the change of ferrite to austenite, hence averting martensite production at grain boundaries. This region demonstrates significant ferrite grain development and a refined distribution of precipitates. The microstructure of CGHAZ exhibits these features. At elevated welding currents, where heat input is increased, the ferrite grain size in this region is noted to be bigger (Figure 4c). Departing from the FZ line results in the formation of ICHAZ with both ferritic and austenitic microstructures (Kou, 2003). Austenite transition transpires along ferrite grain boundaries, subsequently converting to martensite upon cooling, yielding greater hardness than the base material. The production of austenite at high temperatures inhibits grain growth in SS 430, leading to grain pinning at the grain borders. SCHAZ is a slender area beneath the $\delta + \gamma$ zone characterized by an extremely thin grain structure. The FZ region exhibits an acicular ferrite and martensite structure (Figure 6d). Another investigation indicated the occurrence of intergranular carbide precipitation, suggesting that mostly chromium-rich carbides formed in unstabilized ferritic stainless steel alloys, such as SS 430 (Lippold & Kotecki, 2005).

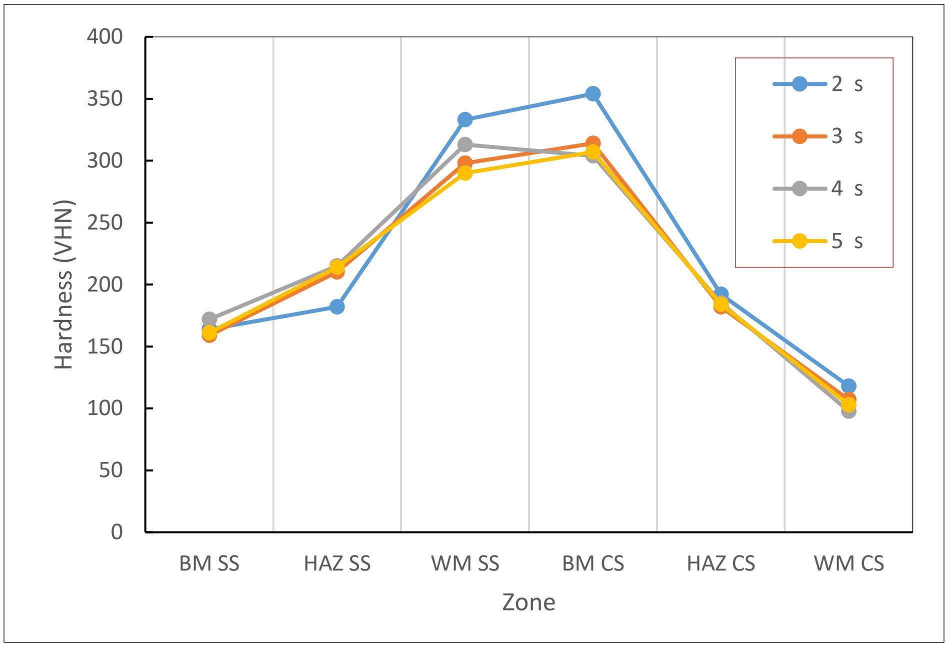

FIGURE 5. *Hardness profile of dissimilar joint of spot welding at various welding time*

The hardness profile quantifies the differences in mechanical properties along the weld seam, which are influenced by its microstructure. The hardness profile of the joint at the interface of SS 430 and carbon steels is illustrated in Figure 5, which delineates three regions: FZ, HAZ, and BM. The production of martensite, a phase harder than ferrite and austenite, results in the FZ exhibiting a higher hardness value than both BMs. Due to the development of a non-equilibrium phase, both carbon steel and SS 430 generally exhibit greater HAZ hardness than BMs. Comparable results from another study conducted by Rajak et al. (2023) reveal that HAZ and FZ exhibit greater hardness values than BM, with FZ being the hardest. Nevertheless, SCHAZ exhibits more softness than BM due to the substantial tempering caused by the increased concentration in HAZ. Additional studies indicated reduced hardness in the HAZ of ferritic stainless steel 409 L, likely due to grain coarsening (A. Kumar et al., 2018). Notably, the hardness adjacent to the FZ/HAZ on the SS 430 side surpasses that of the Carbon steel side. Additionally, the hardness values in the FZ, resulting from shorter welding time, exhibit higher hardness than those from lower currents, likely due to their finer microstructure.

Figure 6a illustrates the load-displacement characteristics of the dissimilar TIG spot welding junction. The load-displacement diagram illustrates a joint's capacity to endure maximal loads, followed by a dramatic decline in the diagram upon initiating and propagating the first fracture. The extent of load reduction is contingent upon the propagation of fractures from the joint until the complete separation of the two plates. Additionally, there is an increase in the extension of the peak load, indicating that the energy absorption from the joint, shown as the area under the curve up to the peak load, also rises (Pouranvari, 2011).

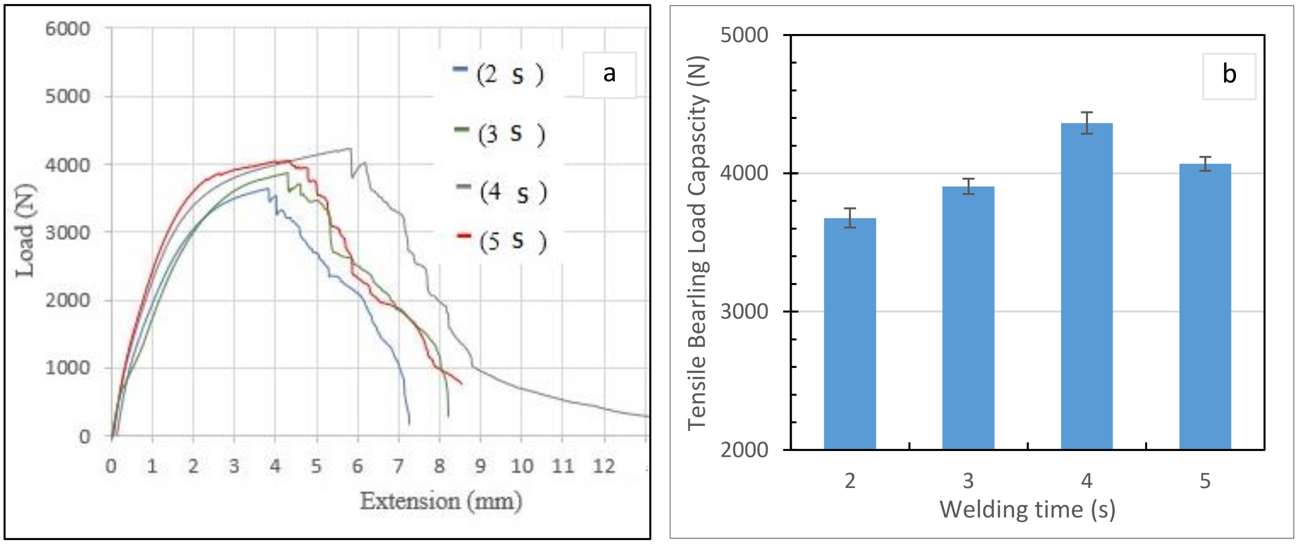

FIGURE 6. *The load-displacement curve of the dissimilar joint of CS/SS430 at various welding times, (b) the effect of welding time on the tensile bearing load capacity (peak load)*

Figure 6b illustrates the correlation between welding time and the mechanical properties of the weld. The tensile load capacity increases as the welding time increases from 2 seconds to 4 seconds, with the highest load capacity observed at 4 seconds (around 4300 N). Beyond 4 seconds, however, the load capacity decreases slightly at 5 seconds, dropping to around 4000 N. The peak load is exacerbated by the increased bonding area of the sheets up to a certain point because of the increased weld time. The larger and more robust weld zone provides better fusion, which improves the tensile load capacity. A larger FZ dimension significantly increases the bonding area between seat sections. As a result, the nugget's resistance to rotation increases, necessitating a greater force to accomplish the ultimate tensile tension at the point of failure in the base metal for the pullout failure mode. However, the peak load decreases at loner welding time (5 s) despite the largest welding zone. The shape and size of the weld zone significantly affect the joint's peak load capacity. With moderate welding times (4 s), the weld achieves an optimal balance in size and shape, resulting in maximum load capacity. However, when welding time is too long (5 s), the excessive heat input can reduce strength by inducing unwanted microstructural changes in the HAZ, such as grain coarsening or forming brittle phases. The TLBC of this dissimilar metal TIG spot welding is lower than that of similar metal TIG spot welding joints of ferritic stainless steel (A. Kumar et al., 2018) and duplex-precipitate (DP) stain steel (Rajak et al., 2023) due to their microstructural aspects and dimension.

The fracture surface of the welds and the failure mode of each joint were analyzed following the tensile-shear testing. The interfacial failure (IF) and pullout failure (PF) modes are the two primary distinguishing modes in which spot weld joints fail (Chao, 2003; Pouranvari & Marashi, 2010; Pouranvari et al., 2011). Interfacial failure was not detected in any of the samples examined in this investigation, and all failed in PF mode. The results align with previous research conducted by (Nugroho et al., 2024) which found that all TIG spot welding joints without heat treatment experienced pull out failure at the weld boundary area and the HAZ area where grain coarsening occurred. The hardness profile as presented by Figure 5, reveals the relationship between welding time and failure modes in spot TIG welds. In the base metal (BM) regions, hardness remains low, indicating minimal impact from welding. In the heat-affected zone (HAZ), hardness peaks at 2–4 seconds of welding due to rapid heating and cooling, making this region prone to brittle fracture under tensile loads. The weld metal (WM) shows moderate hardness, retaining some ductility. At 5 seconds, overheating reduces hardness across all zones, particularly in the WM, leading to grain coarsening and a shift to ductile failure. This analysis underscores the importance of optimizing welding time to balance strength and ductility, as shorter times result in brittle failure in the HAZ. In comparison, longer times reduce overall joint strength.

Figure 7(a) illustrates a typical PF mode wherein nugget extraction from SS 430 sheet occurs. Figure 7b demonstrates the surface failure of SS 430 at the welding zone boundary (Figure 7(c) and HAZ (Figure 7d) due to excessive particle coarsening. It can be seen that the transgranular failure took place in the coarsening ferritic phase. Silva et al. (2023) stated that the ferritic stainless steel's HAZ exhibited particulate growth compared to the base metal. The weld thermal cycle also detected the chi and sigma phases. The brittleness of the ferritic SS has been known to be associated with the sigma phase. Furthermore, the notch durability of as-welded 430 stainless steel is subpar (Kou, 2003) due to excessive grain coarsening.

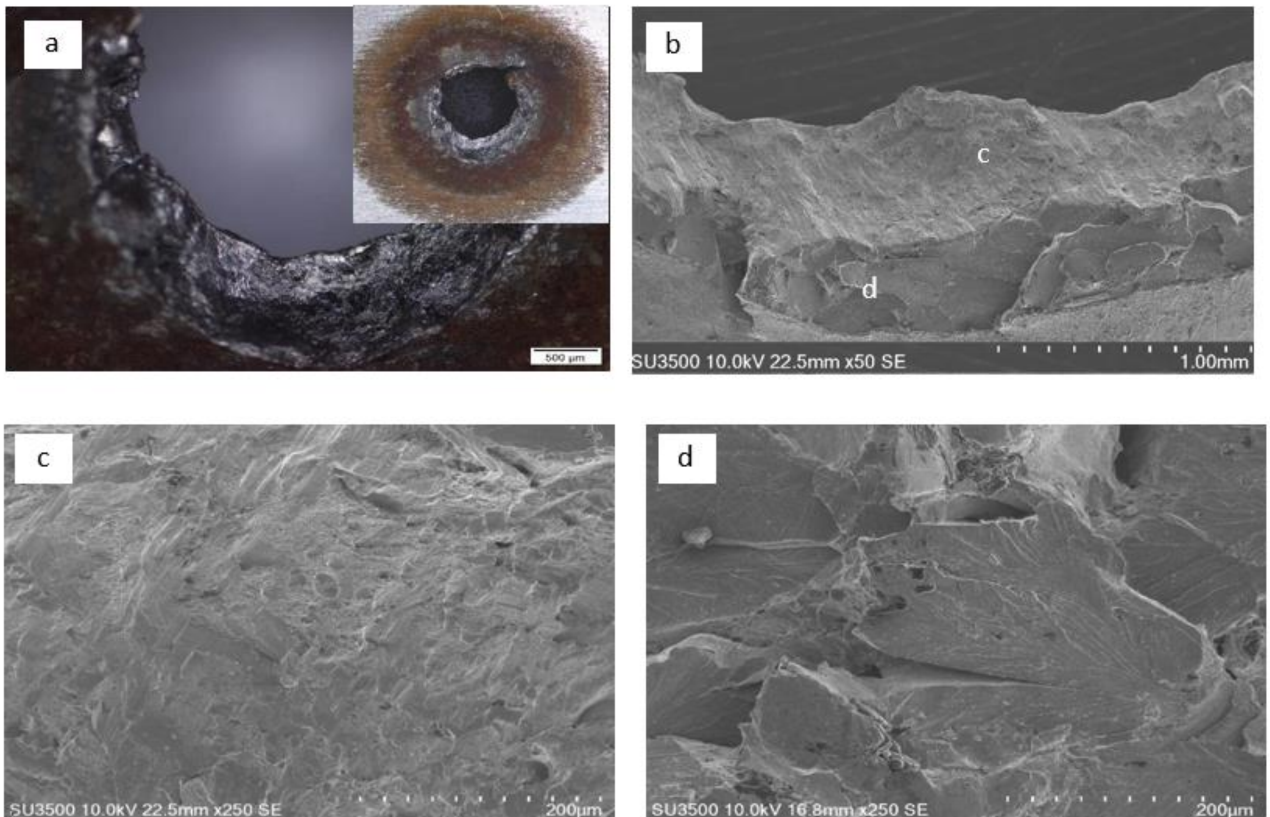

FIGURE 7 *(a) A typical PF mode of the welded joint at 2 second welding time, insert the PF failure of SS430, SEM micrograph of (b) PF at SS430 sheet,(c) failure at welding zone boundary (d) failure at CGHAZ.*

CONCLUSION

The study effectively demonstrated the successful joining of dissimilar metals, SS430 and low-carbon steel, by TIG spot welding. The welding time parameter influences the TLBC of the welded connection, resulting in an increase to 4367 N when the welding time escalates from 2 s to 4 s and then decreases at 5 s welding time. The welding process leads to a substantial increase in grain size within the heat-affected zone (HAZ) of the SS430 sheet compared to that of BM, resulting in brittleness and the occurrence of pullout mode failure in all welded joints within the coarse-grained HAZ. Post-weld heat treatment or an optimal welding time is crucial for achieving maximum strength without compromising the material's microstructure. Although the study achieved significant results, it does not fully address certain limitations, such as potential variability in experimental conditions. To build upon these findings, further investigations could focus on the influence of additional welding parameters, such as current intensity or electrode geometry, to optimize weld quality and expand the scope of industrial applications.

ACKNOWLEDGEMENT

The author expresses gratitude to the laboratory personnel and colleagues of the Mechanical Engineering Department at Universitas Muhammadiyah Yogyakarta for their help during the project.

REFERENCES

Akkaş, N., Ferik, E., İlhan, E., & Aslanlar, S. (2016). The effect of welding current on nugget sizes in resistance spot welding of spa-c steel sheets used in railway vehicles. *Acta Physica Polonica A*, *130*(1), 142-144. https://doi.org/10.12693/APhysPolA.130.142

Alizadeh-Sh, M., Marashi, S., & Pouranvari, M. (2014). Resistance spot welding of AISI 430 ferritic stainless steel: phase transformations and mechanical properties. *Materials & Design (1980-2015)*, *56*, 258-263. https://doi.org/10.1016/j.matdes.2013.11.022

Chao, Y. (2003). Failure mode of spot welds: interfacial versus pullout. *Science & Technology of Welding & Joining*, *8*(2), 133-137.

Echezona, N., Akinlabi, S.A., Jen, T.C., Fatoba, O.S., Hassan, S., Akinlabi, E.T. (2021). Tig Welding of Dissimilar Steel: A Review. In: Awang, M., Emamian, S.S. (eds) Advances in Material Science and Engineering. Lecture Notes in Mechanical Engineering. Springer, Singapore. https://doi.org/10.1007/978-981-16-3641-7_1

Faozi, S. (2015). *The effect of electric current and holding time on mechanical properties of TIG-Spot welding joint of dissimilar materials between steel and aluminum alloy*. [Universitas Sebelas Maret]. Surakarta, Indonesia.

Kou, S. (2003). Welding metallurgy. *New Jersey, USA*, *431*(446), 223-225.

Kumar, A., Sharma, G., & Dwivedi, D. K. (2018). TIG spot weld bonding of 409 L ferritic stainless steel. *International Journal of Adhesion and Adhesives*, *84*, 350-359. https://doi.org/10.1016/j.ijadhadh.2018.04.012

Kumar, K., Mohan, P., & Masanta, M. (2018). Influence of welding current on the mechanical property of 3 mm thick commercial 1050 aluminium butt joint weld by AC-TIG welding method. *Materials Today: Proceedings*, *5*(11), 24141-24146. https://doi.org/10.1016/j.matpr.2018.10.208

Lippold, J. C., & Kotecki, D. J. (2005). *Welding metallurgy and weldability of stainless steels*. John Wiley and Sons, Inc.

Madesh, S., Arul, T., & Perumal, V. (2022). Advances in welding techniques for similar and dissimilar materials. In *Advanced Manufacturing Techniques for Engineering and Engineered Materials* (pp. 183-197). IGI Global.

Mallick, P. K. (2020). *Materials, design and manufacturing for lightweight vehicles*. Woodhead publishing.

Nugroho, A. W., Rahman, M. B. N., & Mahmudi, F. (2024). The effect of welding current on the tensile load capacity of dissimilar metal carbon steel-Stainless steel TIG-spot welded joint. *AIP Conference Proceedings*, *3115*, 040009. https://doi.org/10.1063/5.0207563

Pouranvari, M. (2011). Effect of welding parameters on the peak load and energy absorption of low-carbon steel resistance spot welds. *International Scholarly Research Notices*, *2011*. https://doi.org/10.5402/2011/824149

Pouranvari, M., & Marashi, S. (2010). On the failure of low carbon steel resistance spot welds in quasi-static tensile–shear loading. *Materials & Design*, *31*(8), 3647-3652. https://doi.org/10.1016/j.matdes.2010.02.044

Pouranvari, M., Marashi, S., & Safanama, D. (2011). Failure mode transition in AHSS resistance spot welds. Part II: Experimental investigation and model validation. *Materials Science and Engineering: A*, *528*(29-30), 8344-8352. https://doi.org/10.1016/j.msea.2011.08.016

Rajak, B., Kishore, K., & Mishra, V. (2023). Investigation of a novel TIG-spot welding vis-à-vis resistance spot welding of dual-phase 590 (DP 590) steel: Processing-microstructure-mechanical properties correlation. *Materials Chemistry and Physics*, *296*, 127254. https://doi.org/https://doi.org/10.1016/j.matchemphys.2022.127254

Shrivas, S. P., Vaidya, S. K., Khandelwal, A. K., & Vishvakarma, A. K. (2020). Investigation of TIG welding parameters to improve strength. *Materials Today: Proceedings*, *26*, 1897-1902. https://doi.org/10.1016/j.matpr.2020.02.416

Silva, Y. C. d., Andrade, T. C., Júnior, F. O., Sousa, A. B. F., dos Santos, J. F., Marcondes, F., Miranda, H., & Silva, C. (2023). Numerical investigation of the influence of friction stir welding parameters on the microstructure of AISI 410S ferritic stainless steel joints. *Journal of Materials Research and Technology*, *27*, 8344-8359. https://doi.org/10.1016/j.jmrt.2023.11.054

Singh, L., Singh, R., Singh, N. K., Singh, D., & Singh, P. (2013). An evaluation of TIG welding parametric influence on tensile strength of 5083 aluminium alloy. *International Journal of Mechanical Aerospace, Industrial and Mechatronics Engineering*, *7*(11), 1262-1265.

Zhou, K., & Cai, L. (2014). Study on effect of electrode force on resistance spot welding process. *Journal of Applied Physics*, *116*(8), 084902. https://doi.org/10.1063/1.4893968